An experimental study of the effects of density and viscosity contrasts on macrodispersion in porous media

V. Kretz,[1] P. Berest, J. P. Hulin, and D. Salin

Laboratoire FAST, UMR 7608, Universites Paris 6, Orsay, France

Received 11 February 2002; revised 31 October 2002; accepted 31 October 2002; published 13 February 2003.

[1] We study the vertical miscible displacements of two fluids of different densities and/or viscosities in two model porous media, constructed using different arrangements of blocks of packed glass beads with different sizes. The two configurations have the same permeability distributions but different spatial arrangements and structural features. Time variations of the mean fluid concentration in different sections along the samples are monitored by an acoustic technique. For stable viscosity or density contrasts, the spreading of the displacement front is predominantly macrodispersive. For fluids of the same viscosity but different densities, the macrodispersivities approach at large velocities, where the displacement is stable, the passive tracer limit, $l_{d\infty}$, which is controlled only by the heterogeneity of the medium. This is true, regardless of the density contrast. At lower velocities, where gravity instabilities can exist, the normalized dispersivities $l_d/l_{d\infty}$ vary exponentially with the normalized flow rate, with opposite exponents in the stable and unstable configurations. These results are compared to existing theoretical works based on stochastic approaches and linear stability analyses. *INDEX TERMS:* 1829 Hydrology: Groundwater hydrology; 1832 Hydrology: Groundwater transport; 1869 Hydrology: Stochastic processes; 5114 Physical Properties of Rocks: Permeability and porosity; 5139 Physical Properties of Rocks: Transport properties; *KEYWORDS:* heterogeneities, instability, miscible, dispersion, acoustics, buoyancy

Citation: Kretz, V., P. Berest, J. P. Hulin, and D. Salin, An experimental study of the effects of density and viscosity contrasts on macrodispersion in porous media, *Water Resour. Res., 39*(2), 1032, doi:10.1029/2001WR001244, 2003.

1. Introduction

[2] Porous media heterogeneity is a key factor for the spreading and displacement of fluids in the subsurface. Its understanding is of practical interest to such fields as hydrology, petroleum and environmental engineering. Heterogeneities create preferential flow channels, which greatly enhance pollutant spreading. Conversely, low permeability zones are often bypassed and act as traps for pollutants. Studies based on stochastic continuum approaches [*Dagan*, 1982, 1984, 1987, 1989; *Gelhar and Axness*, 1983; *Rubin*, 1990] have significantly improved our understanding of the effect of heterogeneity on the macrodispersion of passive tracers (namely of tracers of constant density or viscosity and which do no get adsorbed on the pore walls): these studies allow one to relate macrodispersion to the statistics of the permeability field. State-of-the-art reviews of these works are given by *Hsu* [1999, 2000]. A related important issue (although not as thoroughly investigated) is the influence of density and/or viscosity contrasts on the macrodispersion of a non-passive tracer. A number of authors [*Hickernell and Yortsos*, 1986; *Homsy*, 1987; *Bacri et al.*, 1992; *Manickam and Homsy*, 1995; *Loggia et al.*, 1995] have used linear stability analyses to obtain criteria on viscosity and/or density contrasts that lead to the development of viscous and/or gravitational fingering instabilities. Except for *Liu and Dane* [1996] and *de Wit and Homsy* [1997], most of these studies have focused on homogeneous media. A great deal of work has also been done in relation to problems in the unsaturated zone in the immiscible case [see, e.g., *Bauters et al.*, 1998; *Nieber et al.*, 2000].

[3] The interplay between heterogeneity, viscous and density contrasts, and macrodispersion was studied relatively recently. Using a spectral stochastic continuum approach, *Welty and Gelhar* [1991] estimated the macrodispersivity for stable (and unstable) displacements and predicted its spatial dependence by analyzing the transient regime. *Liu and Dane* [1996] analyzed experimentally the influence of gravitational instabilities and grain scale heterogeneity on fluid displacements in a vertical sand column. The results were compared successfully to numerical predictions of 1D and 3D models using the stochastic approaches of *Gelhar and Axness* [1983] and *Welty and Gelhar* [1991]. Experiments by *Tchelepi et al.* [1993] examined the influence of the interaction of heterogeneities with local dispersion and viscosity gradients on miscible fluid displacements. In higher permeability zones, where fluids flow faster, a favorable viscosity contrast reduces the velocity variations, while an unfavorable one enhances them. This effect has been studied quantitatively by *Loggia et al.* [1996] in the simple case of stratified media with layers parallel to the mean flow.

[1] Also at Institut Francais du Petrole, Rueil Malmaison, France.

0043-1397/03/2001WR001244$09.00

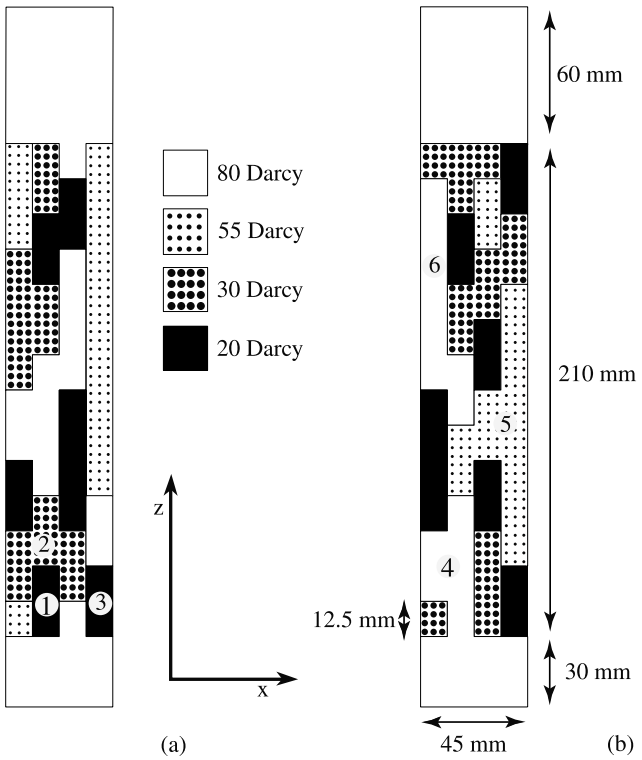

Figure 1. Permeability maps of the two porous media: (a) Medium 1 and (b) medium 2. The permeability is invariant in the *y* direction, perpendicular to the figure plane. Numbers indicated on some of the blocks are used below for the description of some flow paths.

[4] In the present paper, the experimental study of *Loggia et al.* [1996] is extended to heterogeneous media of more complex geometries. For this purpose, patchworks of parallelepiped porous blocks of different permeabilities have been used. Each block consists of an unconsolidated packing of monodisperse glass beads. Two samples, with 56 blocks and the same permeability distribution, but with different spatial arrangements were constructed (Figure 1). The miscible displacement of one fluid by another in the two samples was analyzed with an acoustic technique and the time and spatial variations of the concentration profiles were investigated. The objective is to determine experimentally the interaction between heterogeneity and density or viscosity contrasts, for both stable and unstable configurations, and to assess their effects on macrodispersion. In the following, experiments with fluids of same viscosity and with a stabilizing density contrast will be first discussed: in this case, spreading may be considered as dispersive at the macroscopic scale. Then, experiments will be reported for the case of destabilizing density contrasts and of fluids of the same densities but different viscosities. The dependence of the corresponding macrodispersivity on the flow velocity and the density contrast will then be compared to the theoretical models of *Welty and Gelhar* [1991] and *Hickernell and Yortsos* [1986].

2. Experimental Setup and Procedure

2.1. Experimental Samples

[5] Patchwork-like porous media consisting of parallelepiped cells of dimensions 300 × 45 × 45 mm^3, and bounded by transparent walls were constructed as described below. This technique was already successfully applied by *Loggia et al.* [1996] to create layered porous media, with layers parallel to the flow extending along the full sample length. The permeability of each layer deduced from the experiments corresponded well to the expected value and no permeability anomaly occurred at the interface between blocks (layers).

[6] The porous medium was first partitioned into 4 parallel compartments of identical width using thin vertical spacer plates parallel to the *y*-*z* plane (Figure 1). The compartments were then slowly filled with successive layers of glass beads, of diameters which may vary from one layer to the next and from one compartment to the other (Figure 1). The spacers were progressively raised during the filling process so that they will induce only small local rearrangements, upon their ultimate removal. Horizontal interfaces between layers of different permeabilities were shifted vertically between successive compartments in a brick wall-like geometry.

[7] The 56 elementary blocks are all parallelepipeds of dimensions 12.5 × 45 × 11 mm^3. Each elementary block has a given mean grain size (and therefore permeability), with a porosity which is the same for all blocks ($n \simeq 40\%$). We used 4 sizes of glass beads, whose diameter ranges were 125–150, 150–200, 200–250 and 250–300 μm, respectively, giving rise to permeability values of 20 ± 2, 30 ± 5, 55 ± 7 and 80 ± 8 Darcy (10^{-12} m^2), respectively. The blocks span the thickness of the sample along the *y* direction, hence the global permeability distribution is effectively two–dimensional. Two different block arrangements, with identical statistical probability distributions, were used to study the influence of the spatial permeability distribution. The layout of the blocks in the two samples (referred to as samples 1 and 2) is shown in Figure 1.

2.2. Fluids and Flow Experiments

[8] Miscible displacement experiments were performed in the two samples at several constant flow rates, using water-glycerine and water-sugar mixtures. Adjusting the volume fraction (ϕ) of the solute in each mixture provides fluids with the required density and viscosity. Four particular solutions with the physical properties listed in Table 1 were used.

[9] The properties of the mixtures were measured with an accuracy of 0.2 kg m^{-3} in density and 10^{-4} Pa s in viscosity. The values in Table 1 are consistent with the ones reported in the work of *Weast and Astle* [1980]. For the displacement experiments with pairs of fluids of the same viscosity but different densities, we used fluids 1 and 3. For displacements of fluids of the same density and different

Table 1. Physical Properties of Solutions Used in the Experiments[a]

Reference	Solute	ϕ	μ, Pa s	ρ, kg m^{-3}	V, m s^{-1}
Fluid 1	sugar	38	5.3×10^{-3}	1166	2030
Fluid 2	sugar	32	3.75×10^{-3}	1137	1995
Fluid 3	glycerine	48	5.4×10^{-3}	1120	2140
Fluid 4	glycerine	54	7.5×10^{-3}	1136	2180

[a]Here ϕ is concentration of solute in water, μ is viscosity, ρ is density, and V is sound velocity of the solution-saturated packed beads.

viscosities we used fluids 2 and 4. For further use, we note that the various models need expressions for the concentration dependence of viscosity and density. Fitting the variations of viscosity with an exponential led to $\beta = d\ln(1/\mu)/dC = 0.7$ for the mixtures of fluids 2 and 4. Density variations with concentration were found to be almost linear, leading to first-order to $\alpha = d\ln(\rho)/dC \simeq d\rho/\rho_0 dC = 0.040$ for the mixtures of fluids 1 and 3. The mean flow velocity ranged over two orders of magnitude (between v = 6 mm/h (=0.144 m/d) and v = 500 mm/h (=12 m/d)). In the above, v is the interstitial velocity (or mean pore velocity), whereas $q = v\,n$ is the Darcy (or superficial) velocity. Two experiments were performed for each fluid pair (1, 3 and 2, 4) at each flow rate. A vertical flow configuration was used to avoid gravity override problems. Injections were performed in the upwards direction. Under these conditions, one of the displacements is stable, whereas the other is unstable.

2.3. Concentration Measurements Using Acoustics

[10] The concentration C is determined from measurements of the sound velocity in the sample. The sound velocity depends solely on the effective compressibility and density of the fluid-saturated porous media, whereas sound attenuation depends on viscous dissipation [*Geertsma and Smit*, 1961; *Salin and Schon*, 1981; *Bacri et al.*, 1991; *Berest et al.*, 1999; *Hulin and Salin*, 1999]. For fluid mixtures such as those used in our experiments, the sound velocity depends on the relative concentration of the fluids saturating the porous medium. Sound velocities of the saturated bead pack are listed in Table 1. The acoustic technique is implemented by means of an acoustic scanner measuring, at a fixed height z, the transit time of sound along 10 propagation paths parallel to the x direction and spaced by 4 mm along the y direction, and along 10 propagation paths parallel to the y direction; 20 pairs of transducers inserted on a ring-shaped assembly were used for that purpose. The typical transit time variation for the pairs of fluids used is less than 1 μs; the accuracy of the measured transit time is better than 10 ns [*Hulin and Salin*, 1999]. Within experimental error, the relation between the relative concentration C of the two fluids averaged along the propagation path and the measured sound velocity is linear, which allows to determine C with an accuracy of better than 0.01. The spatial resolution is of the order of the size of the transducers, i.e., 2 mm along x or y and 10 mm along the z axis.

[11] The transducer assembly can be displaced vertically along the z axis. Measurements were performed in 17 cross sections spaced vertically in intervals of 15 mm and located at distances from the injection plane ranging from 22.5 to 262.5 mm. As noted, at a given height, the mean sound velocity is measured along 10 paths parallel to the x direction and along 10 paths parallel to the y direction. The full cycle of measurements requires 30 s and is repeated at regular time intervals, providing a total of 340 time variation curves for each experiment. After an experiment is completed, the corresponding variations of the relative concentrations are obtained by normalizing these curves between values obtained at the same coordinates (x, z) before and long after the displacement. Since the permeability distribution of the sample is invariant along y, the relative concentration of the two fluids should likewise be invariant, at least for stable displacements. This is checked by comparing sound velocity values obtained at a given height with the 10 transducers, which measure sound propagation along x, thus averaging out the effect of the heterogeneities. As in the previous experiments of [*Berest et al.*, 1999], the relative concentration values measured along the various paths parallel to x are the same, except in very unstable displacements: these common values correspond to the mean concentration $\overline{C}(z, t)$ at z and t. Transducer pairs measuring sound propagation along the y axis map the fluid distribution in the different blocks. This allows one to obtain at a given time a 17 × 10-pixel "image" of the normalized relative concentrations of the two fluids in the sample. Such images are shown in Figure 2; the relative concentration $C(x, z, t)$ is coded into 256 grey levels with black corresponding to the displaced fluid and white to the injected one.

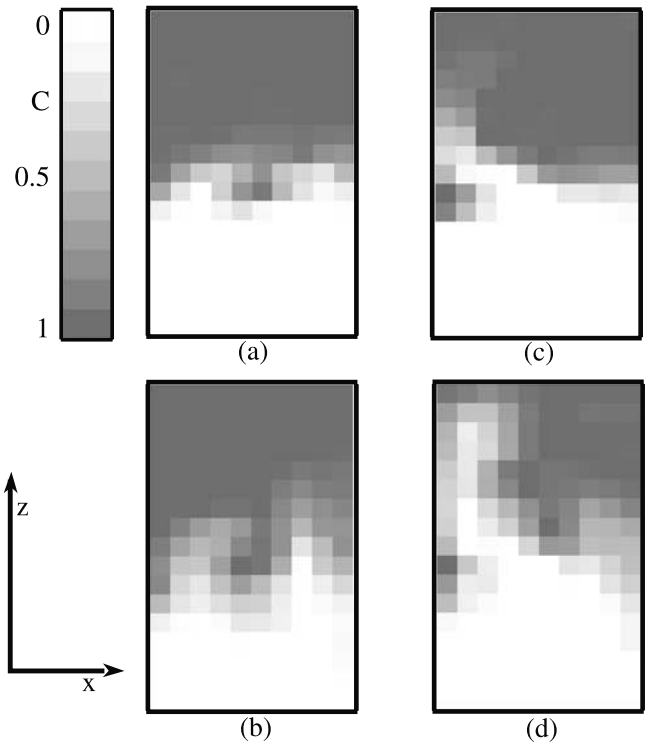

Figure 2. Snapshots of fluid displacements in the two porous media (v = 60 mm/h, $\Delta\rho = \pm 46$ kg m^{-3}): (a) medium 1, stable flow, (b) medium 1, unstable flow, (c) medium 2, stable flow, and (d) medium 2, unstable flow. Shading levels characterize the mean relative concentration $\overline{C}$ of the injected fluid in the corresponding pixel (see gray scale at the top left). The field of view (45 × 210 mm) corresponds to the brick wall part of the sample (scales are different along x and z for better legibility).

2.4. Acoustic Images of Fluid Displacements in Various Flow Configurations

[12] Figures 2a–2d display examples of the maps of the concentration distributions obtained in both samples. By comparing Figures 2a and 2b and Figures 2c and 2d, respectively, one observes that, for both samples, the dis-

placement front is broader in the direction parallel to the mean flow in the unstable flow configuration, compared to the stable one. While their amplitude is very different in the two cases, indentations of the front appear at the same places, implying that they are closely related to the underlying permeability field.

[13] In particular, a large finger-like structure is observed for sample 2 (Figures 2c and 2d). It is associated to a sequence of regions of high permeability (numbered 4, 5, and 6 in Figure 1) which provides a higher velocity channel in the sample. Front deformations are smaller in sample 1: in this case, a set of low permeability blocks (numbered 1, 2 and 3 in Figure 1) extending across the sample acts as a barrier, thus distributing the flow more evenly.

[14] Acoustic images provide useful qualitative pieces of information on preferential flow paths and dead zones. The measurements of the average concentration, $\overline{C}$ (z, t), so obtained will be used next for a quantitative analysis. Before describing the experiments and their analysis, it is necessary to provide a brief theoretical background.

3. Theoretical Background

3.1. Dispersion of a Passive Tracer

[15] *Gelhar and Axness* [1983] used a stochastic approach to study the dispersion of a passive tracer (same densities and viscosities) in the limit of small perturbations and with some restrictive conditions on the heterogeneities of the permeability field. They found that asymptotically, the mean concentration $\overline{C}(z, t)$ satisfies the classical 1D advection-dispersion equation:

$$\frac{\partial \overline{C}(z,t)}{\partial t} + v\frac{\partial \overline{C}(z,t)}{\partial z} = D\frac{\partial^2 \overline{C}(z,t)}{\partial z^2} \tag{1}$$

in which D is the longitudinal dispersion coefficient. For a step-like variation of the mean tracer concentration $\overline{C}(0, t)$ at the sample inlet, the concentration profile is:

$$\overline{C}(z,t) = \frac{1}{2}\mathrm{erfc}\left(\frac{z - vt}{2\sqrt{Dt}}\right) \tag{2}$$

Thus, the width of the transit time distribution through a given section of the sample increases with the mean transit time, $\bar{t}$, from the beginning of the injection, as $\sqrt{\bar{t}}$. Moreover, the dispersion coefficient D is related to $\bar{t}$ and to the variance $\overline{\Delta t^2}$ of the transit time by:

$$\overline{\Delta t^2} = \frac{2D\bar{t}}{v^2} = \frac{2l_d\bar{t}}{v} \tag{3}$$

in which the length $l_d = D/v$ is the dispersivity ($l_d = A_{11}^0$ in the work of *Gelhar and Axness* [1983]). When the system reaches dispersive behavior, the dispersivity was shown by *Gelhar and Axness* [1983] to be proportional to the correlation length of the system and the variance of the log permeability.

[16] The method for passive tracer dispersion was subsequently extended by *Welty and Gelhar* [1991] to fluids of different densities and/or viscosities. They obtained the following expression for the effective dispersivity

$$A_{11} = A_{11}^0 e^{-2a_1} \tag{4}$$

where

$$a_1 = \beta G_1 \bar{z}\left[\frac{1}{\gamma} + \frac{d\rho_l}{d\mu_l}\frac{k_l g}{q}\right] \tag{5}$$

Here, G_1 is the macroscopic concentration gradient $\partial\overline{C}/\partial z$ of the two fluids, q is the mean superficial velocity, $\beta = \partial(ln\,\mu)/\partial\, C$, k_l, ρ_l and μ_l represent respectively the geometric means of the permeability, density and the inverse of the viscosity and γ is a flow factor, taken equal to 1 at the leading order for which this theory is valid [*Chin*, 1997; *Hsu*, 1999, 2000; L. Talon et al., Lattice BGK simulations of macrodispersion in heterogeneous porous media, submitted to *Water Resources Research*, 2002]. We note the following: (1) equation (5) predicts a length-dependent dispersivity. (2) The permeability heterogeneity influences only the prefactor of the exponential, while viscosity and density contrasts enter only in the argument of the exponent. In fact, the prefactor should reduce to the dispersivity for the passive tracer case. (3) The product of the dispersivities of two displacements, one stable and one unstable (with equal in magnitude arguments but different signs in the exponent) should be a constant. These theoretical findings will be tested below in the experiments.

[17] Equation (5) can be simplified by assuming an exponential dependence of viscosity on the relative concentration C, so that $\ln \mu$ varies linearly with C, in which case $\ln M = \partial \ln\mu/\partial C = \beta$. Here M is the ratio of the viscosities of the displaced and injected fluids (with $M < 1$ in the stable configuration). Assuming also a linear variation of the density with C, $\partial\rho/\partial z$ can be replaced by $\Delta\rho\partial\overline{C}/\partial z$ where $\Delta\rho$ is the density difference between the displaced and injected fluids. Then (5) takes the approximate form:

$$a_1 = G_1\bar{z}\left[\frac{\Delta\rho k_l g}{q\mu_l} - \ln M\right] \tag{6}$$

Due to the assumed respective exponential and linear dependencies of viscosity and density on concentration, only their mean values or their values appear in the formula. The influence of the detailed structure of the mixing zone is implicit in the $\partial\overline{C}/\partial z$ term.

[18] Note parenthetically, that the first term in the bracket in (6) is the gravity number B_ν, expressing the ratio of buoyancy to viscous forces:

$$B_\nu = \frac{\Delta\rho g k_l}{\mu q} \tag{7}$$

where q is the Darcy velocity, k_l the geometric mean of the permeability and $g = 9.81$ m s^{-2}. In our experiments, this number varies between $B_\nu = 0.06$ at high flow rates to $B_\nu = 5.3$ at low rates. B_ν^{-1} can also be considered as a normalized Darcy velocity, $B_\nu^{-1} = q/q_c$, in which:

$$q_c = \frac{\Delta\rho g k_l}{\mu} \tag{8}$$

In our experiments, $q_c = 12.7$ mm/h. Alternatively, one can consider B_ν^{-1} as a normalized interstitial velocity, $B_\nu^{-1} = v/v_c$ with $v_c = q_c/n$ ($v_c = 31.7$ mm/h).

[19] The exponential growth (or decay) in (4) does not necessarily require dispersive behavior, but only that per-

turbations are small, so that a linearized theory can be used. In such cases, a linear stability analysis should lead to similar predictions for an exponential rate of growth (or decay). *Hickernell and Yortsos* [1986] applied a linear stability analysis to homogeneous porous media in the absence of small-scale dispersion. In a moving frame of reference, the temporal growth of small perturbations is assumed to be of the form $\exp(\sigma t)$, which in the present context can be replaced by $\exp(\sigma\bar{z}/v)$. This expression is similar to (4). In fact, the maximum growth rate in the short-wave limit was predicted to be

$$\sigma_{max} = \max\left[v\left(\frac{d\ln\mu}{dz} - \frac{k}{\mu q}\frac{d\rho}{dz}\right)\right] \tag{9}$$

[20] Using the same assumptions as above, density and viscosity variations with distance can be written as a function of the concentration gradient and of $\Delta\rho$ and $\ln M$, respectively, leading to:

$$\sigma_{max}\frac{\bar{z}}{v} = \max\left(\bar{z}\frac{\partial\overline{C}}{\partial z}\left[\frac{\Delta\rho g k}{q\mu} - \ln M\right]\right) \tag{10}$$

For our problem, the maximum value corresponds to $C = 0.5$ with $\mu(C = 0.5) = \sqrt{\mu_{dis}\mu_{inj}} = \mu_l$ so that the final expression of $\sigma_{max}\bar{z}/v$ is, within a factor of two, identical to that of a_1 in (6). The difference of a factor of 2 is simply due to the fact that the macrodispersion in the stochastic approach of *Welty and Gelhar* [1991] is obtained as the ensemble average of the product of two perturbations, the exponential parts of which are the same, hence leading to the additional factor of 2.

3.2. Predictions to be Compared Against Experimental Data

[21] In the case of a stabilizing density contrast and of fluids of equal viscosities ($M = 1$), (4)–(6) become:

$$A_{11} = A_{11}^0 \exp(-2G_1\bar{z}B_v) \tag{11}$$

implying an exponential variation of dispersivity with B_v (and therefore with $1/q$). Thus the experimental dispersivity l_d should verify:

$$\frac{l_d(B_v)}{l_{d\infty}} = \exp(-2G_1\bar{z}B_v) \tag{12}$$

where $l_{d\infty}$ is the dispersivity in the high velocity limit. If this is to be verified, it would also be in agreement with the fact that a_1 should be independent of the spatial permeability distribution, which should only influence the prefactor A_{11}^0.

[22] Equations (4)–(6) predict very simple relations between dispersivity values obtained in stable and unstable flow configurations. Compare, for instance, dispersivity values obtained at a given velocity and for a pair of fluids of same viscosity but different densities; when the injected and displaced fluid are exchanged, the corresponding values of a_1 become opposite. Therefore the product of the dispersivities in the two configurations at a same Pe value should be independent of Pe and equal to $l_{d\infty}^2$. Similar relations are also expected for pairs of fluids of the same density but different viscosities. To verify these theoretical predictions we need to conduct experiments with unstable density or viscosity contrasts. These are reported and analyzed below. The following present first, experiments with density contrasts, then experiments with viscosity contrasts.

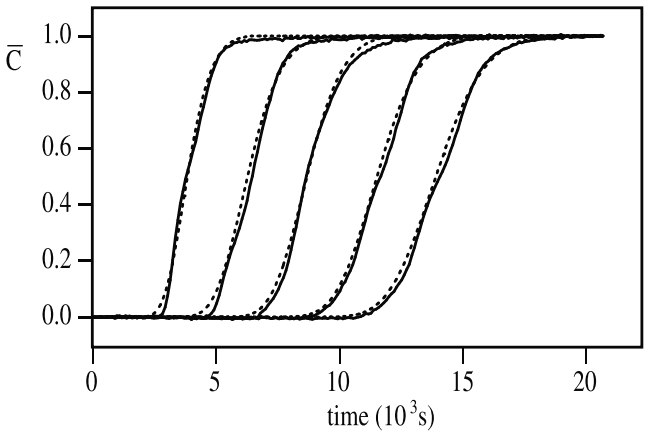

Figure 3. Variation of the mean concentration versus time for porous medium 1 and for stable flow (lighter fluid on top of heavier one) (v = 60 mm/h, $\Delta\rho$ = 46 kg m^{-3}). The curves correspond to sample cross sections at distances from the inlet equal to 37.5, 82.5, 127.5, 172.5 and 217.5 mm, respectively. The dashed lines are experimental fits to the data using (2).

4. Experiments With Density Contrasts

[23] We studied fluid displacements with density contrasts both gravitationally stable and unstable. In the stable configurations, the heavier fluid 1 is injected upwards to displace the lighter fluid 3, initially saturating the medium. The two fluids have the same viscosity, but different density: $\Delta\rho = \rho_{inj} - \rho_{dis} = \rho_1 - \rho_3 = 46$ kg m$^{-3} > 0$ (where ρ_{inj} and ρ_{dis} are the densities of injected and displaced fluids, respectively). For the flow rates involved in these experiments, the Péclet number $Pe = vd/D_m$ varied between $Pe = 0.8$ and $Pe = 70$ (where d is a typical micro-scale taken equal to the average bead size d = 250 μm, and $D_m = 5.\ 10^{-10}$ m^2 s^{-1} is the molecular diffusion coefficient [*Weast and Astle*, 1980]). Under these conditions, convective or mechanical mixing overcomes molecular diffusion [*Hulin and Salin*, 1999]. In this regime, the main forces are buoyancy and viscosity.

4.1. Stabilizing Density Contrast

[24] Figure 3 shows relative variations of the mean concentration $\overline{C}(z, t)$, measured in five sample sections, as a function of time. The acoustic images of Figures 2a and 2c also correspond to experiments of this type. We observe that curves obtained in this stable case are quite smooth. In this finite-length medium, all show an overall S-like shape with the maximum slope (near $\overline{C} = 0.5$) decreasing slowly with distance. These features are similar to those of dispersion curves in homogeneous porous media [*Hulin and Salin*, 1999], where the mean concentration $\overline{C}(z, t)$ satisfies (2). The experimental curves for both samples were well fitted by solutions of (1) (dashed lines in Figure 3). This suggests

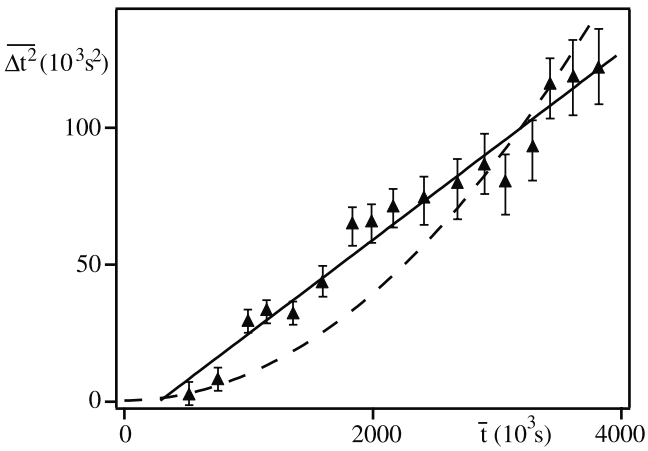

Figure 4. Variance $\overline{\Delta t^2}$ of the transit time through the sample versus the mean value $\bar{t}$ in the stable displacement configuration. Solid line shows linear regression. Dashed line shows parabolic regression.

that the spreading of the displacement front is also dispersive in this case, despite the fact that the medium is of a finite length: this was confirmed by the variations with the distance z of the mean value, $\bar{t}$, and of the variance, $\overline{\Delta t^2}$, of the transit time distribution. These quantities were computed analytically from the parameters of the fitted functions of (2). (From such a fit, we also find that $\bar{t}$ increases linearly (within 2%) with z: the inverse of this slope, which is equal to the mean transit velocity v, is in good agreement with the value computed from the flow rate, the cross section and the porosity.) Figure 4 displays variations of $\overline{\Delta t^2}$ as a function of $\bar{t}$ for the same set of curves as in Figure 3. The data points correspond to sound propagation in a direction parallel to y at 17 different distances along z and at 10 different distances along x. The linear regression corresponds to dispersive spreading of the front $\overline{\Delta t^2} \propto \bar{t}$ and the parabolic to a convective process for which the front width increases linearly with distance (namely, $\sqrt{\overline{\Delta t^2}} \propto \bar{t}$). Clearly, the straight line provides a much better fit to the data points, confirming the dispersive spreading: this allows us to determine through (3) an effective dispersion coefficient D and a dispersivity $l_d = D/v$ (using the slope of the regression line and the experimental value of v).

4.2. Velocity Dependence of the Dispersivity in the Stable Case

[25] Figure 5 displays the dependence of the dispersivities l_{d1} and l_{d2}, respectively, for porous media 1 and 2, as a function of the reduced flow rate, namely of $B_\nu^{-1} = v/v_c$. In both cases, l_d increases with B_ν^{-1}, up to a constant limit $l_{d\infty}$, at which point the influence of gravity becomes negligible. At high rates, viscous effects overcome gravity and at this limit, the problem should correspond to "passive tracer" dispersion. The values obtained for samples 1 and 2 are $l_{d1\infty} \backsimeq 2.5$ mm and $l_{d2\infty} \backsimeq 7$ mm, respectively. This difference mirrors the larger amplitude of the front distortions observed in Figure 2 for sample 2. At low B_ν^{-1}, gravity becomes dominant and l_d decreases significantly.

[26] While the asymptotic dispersivities for the two different permeability arrangements are different, we did not further attempt to extract from them a correlation length and a log permeability variance, as predicted by the passive-tracer theory. While sample 2 does suggest a longer correlation length, which is consistent with the fact that it has more channel-like features, the number of blocks in the system is simply too small, for a statistical theory to be applicable. The so-obtained dispersivities do mirror, however, important permeability heterogeneity features. A more robust analysis, however, is possible for the effect of density and viscous contrasts.

[27] It was noted in (12) that the overall variation of $l_d/l_{d\infty}$ with B_ν should be an exponential, assuming the validity of the linear theory. This relation was well verified by the experimental data (dotted lines in Figure 5) and, for both samples, the best fit is obtained for the same value of $G_1\bar{z} = 1.1$. This is in agreement with the fact that a_1 should be independent of the spatial permeability distribution, which should only influence the prefactor A_{11}^0. It is difficult to determine accurately $G_1\bar{z}$ since the concentration gradient is not constant over the front and $G_1\bar{z}$ varies during the front propagation. Taking $\bar{z} = 250$ *mm* and $\Delta z = 50 - 100$ *mm* gives $G_1\bar{z} \backsimeq 2.5$ to 5. The agreement may be considered as reasonable, in view of the crudeness of these approximations. Also, the two theoretical approaches [*Hickernell and Yortsos*, 1986; *Welty and Gelhar*, 1991] are first-order results, while significant density variations do occur in the present experiments.

4.3. Unstable Density Contrast

[28] Unstable density experiments were performed with the same pair of fluids as previously and at the same Bond numbers, but with the injected and displaced fluids interchanged, resulting in a gravitationally unstable configuration. In the unstable case, the nature of the instability shows up through local distortions of the curves, as shown in Figure 6. The experimental curves were analyzed in the same way as previously (although the precision on the determination of l_d was poorer due to stronger deviations from (2)).

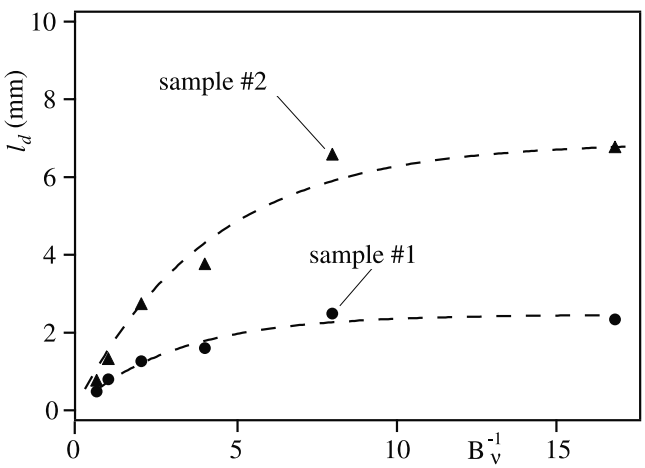

Figure 5. Variation of the dispersivity, l_d, versus the reduced velocity (or the inverse gravity number $B_\nu^{-1} = \mu q/\Delta\rho g k_l$) for buoyancy-stable displacement ($\Delta\mu = 0$, $\Delta\rho = 46$ kg m^{-3}) for medium 1 (solid circles) and medium 2 (solid triangles). Dashed lines show fit of the data with (12) using the corresponding $l_{d\infty}$ of each medium.

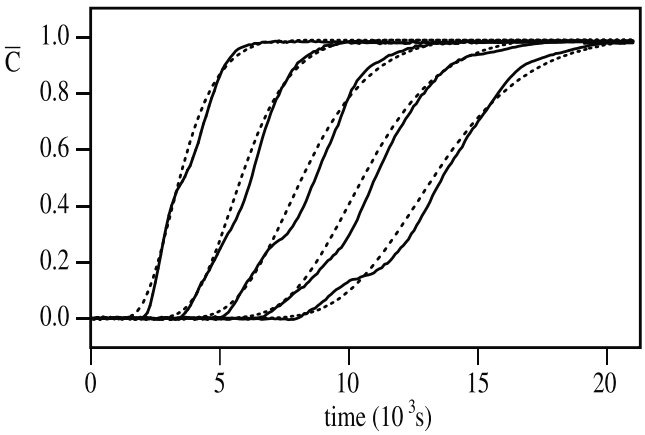

Figure 6. Variation of the mean concentration in different sample cross sections versus time for porous medium 1 and for unstable flow (heavier on top of lighter) (v = 60 mm/h, $\Delta\rho$ = 46 kg m^{-3}). The curves correspond to the same distances from the inlet as in Figure 3. The dashed lines are experimental fits to the data using (2).

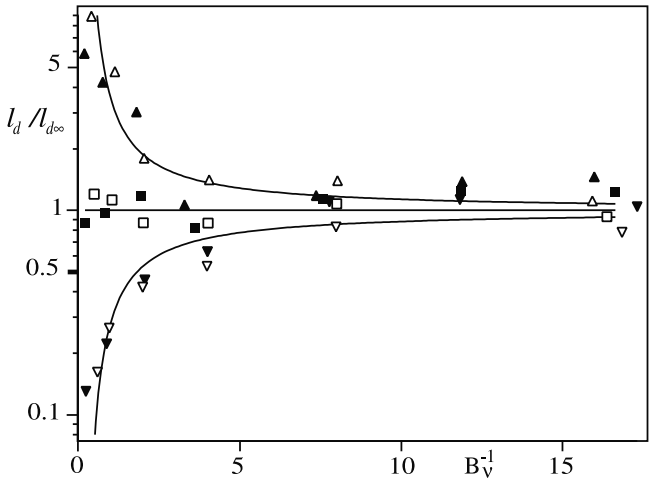

Figure 7. Log linear plot of the dispersivities normalized by their respective asymptotic value $l_{di\infty}$ (at large B_v^{-1}, see Figure 5) for porous medium 1 (open inverted triangles, stable flow; open triangles, unstable flow; open squares, geometrical average) and porous medium 2 (solid inverted triangles, stable flow; solid triangles, unstable flow; solid squares, geometrical average). Solid lines correspond to fits with (12) for both configurations and to the geometrical average of the fits (horizontal).

[29] To test the validity of the theoretical predictions, we show in Figure 7 a log linear plot of the dispersivities of each medium normalized by their own asymptotics $l_{di\infty}(i$ = 1, 2) versus the reduced flow velocity.

[30] One observes that data points corresponding to the two porous media 1 and 2 follow the same variation when normalized in this way. Moreover, for both samples 1 and 2, data points obtained in the stable and unstable configurations at the same Péclet number are symmetrical and vary exponentially with $1/B_\nu$ with opposite arguments (solid lines). The same fit is valid for data points corresponding to both samples, so that the coefficient of B_ν in (12) is the same. Last, the geometric mean $\sqrt{l_{d-stable}(B_\nu) l_{d-unstable}(B_\nu)}$ (squares in Figure 7) is constant and equal to the corresponding value, $l_{di\infty}$, as expected from the small-fluctuation theory.

[31] These results confirm that the parameter a_1 is the same for both samples and that only its sign changes when injected and displaced fluids are interchanged. As expected from the theory, dispersivity values in the unstable case are markedly higher than in the stable configuration at low flow velocities. The difference between the two values decreases as the reduced flow rate increases, both converging towards the same value $l_{di\infty}$ above $B_v^{-1} \backsimeq 20$, where viscous forces dominate.

5. Experiments With Viscosity Contrasts

[32] The next series of experiments was carried out with fluids 2 and 4, which have identical densities but a ratio of 2 between their viscosities. The data acquisition and analysis procedure is the same as in the previous experiments and provides dispersivity values l_{di} (i = 1 or 2) for the two samples studied, for various combinations of flow rates and for stable (M = 0.5) or unstable (M = 2) viscosity contrasts. As above, assuming a linear variation of the variance $\Delta\overline{t^2}$ of the residence time t with the mean value $\bar{t}$ provides a better fit with data points than a quadratic variation (particularly in the stable case). From (4)–(6), then the dispersivity should satisfy the following expression:

$$\frac{l_d}{l_{d\infty}} = \exp 2G_1\bar{z}[lnM] \tag{13}$$

The variations of the normalized dispersivities $l_{d-unstable}/l_{d\infty}$ and $l_{d-stable}/l_{d\infty}$ in medium 1 are plotted in Figure 8 as a function of the Péclet number for M = 0.5 and M = 2 (the Péclet number is used for the horizontal scale since no parameter equivalent to v_c in (8) is available to normalize

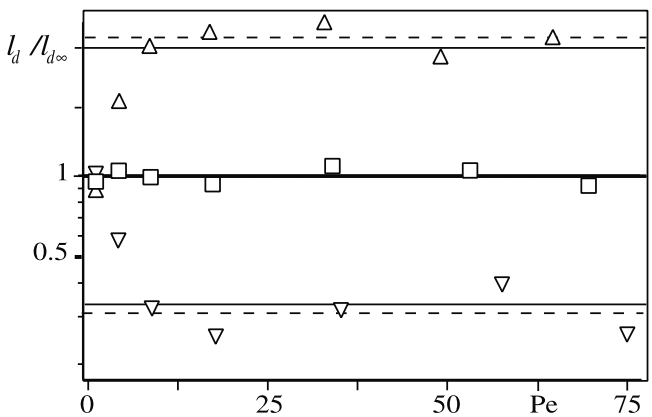

Figure 8. Log linear plots of the variation of the normalized dispersivities versus Pe for stabilizing and destabilizing viscosity contrasts (M = 2 and M = 0.5) in medium 1. Inverted triangles, stable flow, triangles, unstable flow; squares, geometrical average. The horizontal solid lines denote values from (13). Dashed lines show average of the values for Pe > 30.

the velocity). Except at the two smallest flow rates ($Pe = 2.8$ and $Pe = 5.6$), $l_{d-unstable}/l_{d\infty}$ and $l_{d-stable}/l_{d\infty}$ do not depend on Pe. This indicates a mechanical dispersion regime [*Hulin and Salin*, 1999] only associated with the distribution of the flow paths in the medium and independent of the flow rate in the Darcy limit. Such a behavior was also observed in layered porous media [*Loggia et al.*, 1996]. The reference value $l_{d1\infty}$ is that determined in the high velocity limit in the previous series of experiments, assuming that the value of A_{11}^0remains the same.

[33] Equation (13) predicts values of the ratio $l_d/l_{d\infty}$ independent of the flow rate but with opposite signs in the argument of the exponential for $M = 2$ and $M = 0.5$. As above, this can be verified by plotting the dispersivities in logarithmic coordinates: the data points for $M = 2$ and $M = 0.5$ are symmetrical with respect to the horizontal line $l_d/l_{d\infty} = 1$ and well predicted by (13) for $Pe > 6$. The geometric means of the dispersivities measured at the same velocity are also plotted on Figure 8 (squares) and are close to the horizontal line, as expected.

[34] The decrease of the contrast between values in the stable and unstable configurations for $Pe < 6$ is not predicted by the theory: it is likely due to lateral dispersion enhancing the exchange between channels with different flow velocities and/or to residual density contrast effects.

[35] Qualitatively similar results were obtained for sample 2 but the geometric mean $\sqrt{(l_{d-stable}l_{d-unstable})/l_{d2\infty}^2}$ is of the order of 0.85 instead of the theoretical value 1, while the high velocity limit of l_d2 in the stable configuration is lower by 40% than the predictions. This may be an indication of the fact that the large preferential flow channel observed in this sample introduces a bias with respect to the model we have used.

[36] We should note that the relation between macrodispersivities obtained in the two series of experiments (equal-viscosity and equal-density) may be explained from the respective expressions of the terms containing respectively viscosities and densities in (4)–(6) or (10). Viscosity variations appear in these equations through the ln M term, whereas density variations appear through a linear term (in both cases in the argument of the exponential). Thus, the deviation of the dispersivity from the passive tracer value should be the same if both terms have the same value (independent of the uncertainty in evaluating $G_1\bar{z}$). Thus, for $M = 2$, the value of B_ν^{-1} for which buoyancy effects are of the same order of magnitude as the viscous ones should be equal, from (6), to $\ln M = \pm \ln 2 = \pm.7$. For this value of B_ν^{-1}, the normalized dispersivity $l_d/l_{d\infty}$, ($B_\nu^{-1} = 0.7$) in the curves of Figure 7 should be equal to the high velocity limits of the curves of Figure 8 in the stable and unstable cases, respectively. In Figure 7 one can see that this condition is approximately verified.

6. Conclusions

[37] The experimental findings of the present work suggest several important features regarding the influence of viscosity or density contrasts on miscible displacements in porous media. Two controlled heterogeneous samples of same statistical permeability distribution but with different spatial arrangements have been used. Although demonstrated on such model porous media, many of our conclusions should also apply to systems of larger size and different heterogeneity.

[38] A first conclusion is that, in our experimental configuration of a finite system size, the spreading dynamics are dominantly dispersive, certainly for stabilizing viscosity or density contrasts. This allows us to characterize the spreading of the displacement front by a single macrodispersivity parameter.

[39] A second conclusion is the important role played by the passive tracer dispersivity. The measured dispersivity value $l_{d\infty}$ is markedly higher (7 mm) for one sample than for the other (2.5 mm). The limited size of the samples and the small number of blocks does not allow for quantitative comparisons with stochastic theories, as it is doubtful that the asymptotic dispersion limit has been reached. At the same time, the experiments reported here indicate that the spatial structure of the permeability field only influences dispersivity through the high-velocity limit $l_{d\infty}$. For example, the velocity dependence of the normalized dispersivities $l_d/l_{d\infty}$ is the same for both samples (particularly when the viscosities are the same and the densities differ). This implies that at least in the limit considered in our experiments, heterogeneity and density/viscosity contrasts enter as a product of two different terms, one involving the permeability structure and another involving an exponential growth (or decay). In addition, the geometric mean of the two dispersivities measured in a given sample at a same Pe value and with stable and unstable density contrasts is equal to or close to $l_{d\infty}$.

[40] The experimental dependence of $l_d/l_{d\infty}$ on the gravity number can be represented by a simple exponential law ($\exp \pm 2G_1\bar{z}B_\nu$) for fluids of same viscosities and density difference $\Delta\rho$. This law is compatible with expressions inferred from the stochastic model of [*Welty and Gelhar*, 1991] and the stability model of [*Hickernell and Yortsos*, 1986], even though not all conditions required for the application of these models are fulfilled. In the case of equal-density fluids with different viscosities ($M = 2$ and $M = 0.5$), the normalized dispersivities differ in the stable and unstable configurations and are constant for $Pe > 6$. In this case, too, the predictions of the above models are compatible with these results.

[41] Even though full quantitative comparisons between models and experiments cannot be realized due to the limited size of the samples, the present results provide helpful guidelines for analyzing such processes: a good example is the simple relations between dispersivities measured in the stable and unstable configurations and in the passive tracer limit. Future work should evaluate the generality of these results by applying the same experimental approach to systems with a larger number of blocks and different permeability distributions. New theoretical models should also take into account diffusion and transverse dispersivity effects.

[42] **Acknowledgments.** It is a pleasure to acknowledge stimulating discussions with Y.C. Yortsos, M. Le Ravalec, R. Lenormand and B. Noetinger. We also thank Y. Yortsos and N. Rakotomalala for a careful and thoughtful reading of the manuscript. We gratefully thank G. Chauvin, C. Frenois, R. Pidoux and C. Saurine for their technical help. The PhD work of V. Kretz is funded by a CNRS-IFP scholarship. This work is also part of the French National Program of Research in Hydrology (PNRH). All these sources of support are gratefully acknowledged.

References

Bacri, J. C., M. Hoyos, N. Rakotomalala, D. Salin, M. Bourlion, G. Daccord, R. Lenormand, and A. Soucemariadin, Ultrasonic diagnostic in porous media and suspensions, *J. Phys. III France*, *1*, 1455–1466, 1991.

Bacri, J. C., D. Salin, and Y. C. Yortsos, Analyse lineaire de la stabilite de l'ecoulement de fluides miscibles en milieux poreux, *C. R. Acad. Sci. Paris*, *314*, 139–144, 1992.

Bauters, T. W. J., D. A. DiCarlo, T. S. Steenhuis, and J. Y. Parlange, Preferential flow in water-repellent sands, *Soil. Sci. Soc. Am. J.*, *62*, 1185–1190, 1998.

Berest, P., N. Rakotomalala, J. P. Hulin, and D. Salin, Experimental and numerical tools for miscible fluids displacement studies in porous media with large heterogeneities, *Eur. Phys. J. Appl. Phys.*, *7*, 277–289, 1999.

Chin, D. A., An assessment of first-order stochastic dispersion theories in porous media, *J. Hydrol.*, *199*, 53–73, 1997.

Dagan, G., Stochastic modelling of groundwater flow by unconditional and conditional probabilities, 2, The solute transport, *Water Resour. Res.*, *18*, 835–848, 1982.

Dagan, G., Solute transport in heterogeneous porous formation, *J. Fluid. Mech.*, *145*, 151–177, 1984.

Dagan, G., Theory of transport by groundwater, *Annu. Rev. Fluid Mech.*, *19*, 183–215, 1987.

Dagan, G., *Flow and Transport in Porous Formations*, Springer-Verlag, New York, 1989.

de Wit, A., and G. M. Homsy, Viscous fingering in periodically heterogeneous porous media, I, Formulation and linear stability, *J. Chem. Phys.*, *107*, 9609–9618, 1997.

Geertsma, J., and D. C. Smit, Some aspects of elastic wave propagation in fluid-saturated porous solid, *Geophysics*, *26*, 169–181, 1961.

Gelhar, L. W., and C. L. Axness, Three-dimensional stochastic analysis of macrodispersion in aquifers, *Water Resour. Res.*, *19*, 161–180, 1983.

Hickernell, F. J., and Y. C. Yortsos, Linear stability of miscible displacement processes in porous media in the absence of dispersion, *Stud. Appl. Math.*, *74*, 93–115, 1986.

Homsy, G. M., Viscous fingering in porous media, *Annu. Rev. Fluid. Mech.*, *19*, 271–301, 1987.

Hsu, K. C., A general method for obtaining analytical expressions for the first-order velocity covariance in heterogeneous porous media, *Water Resour. Res.*, *35*, 2273–2277, 1999.

Hsu, K. C., General first-order expressions for solute transport in two-and three-dimensional randomly heterogeneous porous media, in *Theory, Modeling, and Field Investigation in Hydrogeology: A Special Volume in Honor of Shlomo P. Neuman's 60th Birthday*, edited by D. Zhang and C. L. Winter, Spec. Pap. Geol. Soc. Am., *348*, 91–104, 2000.

Hulin, J. P., and D. Salin, Acoustical and electrical methods for the study of fluid mixing in porous media, in *Methods in the Physics of Porous Media, Exp. Methods Phys. Sci.*, vol. 35, edited by P. Z. Wong, pp. 425–475, Academic, San Diego, Calif., 1999.

Liu, H. H., and J. H. Dane, Two approaches to modeling unstable flow and mixing of variable density fluids in porous media, *Transp. Porous Media*, *23*, 219–236, 1996.

Loggia, D., N. Rakotomalala, D. Salin, and Y. C. Yortsos, Evidence of new instability thresholds in miscible displacements in porous media, *Europhys. Lett.*, *32*, 633–638, 1995.

Loggia, D., N. Rakotomalala, D. Salin, and Y. C. Yortsos, Phase diagram of miscible displacements in layered porous media, *Europhys. Lett.*, *36*, 105–110, 1996.

Manickam, O., and G. M. Homsy, Fingering instabilities in vertical miscible displacement flows, *J. Fluid. Mech.*, *288*, 75–102, 1995.

Nieber, J. L., T. W. J. Bauters, T. S. Steenhuis, and J. Y. Parlange, Numerical simulation of experimental gravity-driven unstable flow in water repellent sand, *J. Hydrol.*, *231-232*, 295–307, 2000.

Rubin, Y., Stochastic modeling of macrodispersion in heterogeneous porous media, *Water Resour. Res.*, *26*, 133–141, 1990.

Salin, D., and W. Schon, Acoustics of water saturated packed glass spheres, *J. Phys. Lett.*, *42*, L-477–L-480, 1981.

Tchelepi, H. A., F. M. Orr Jr., N. Rakotomalala, D. Salin, and R. Woumeni, Dispersion, permeability heterogeneity and viscous fingering: Acoustic experimental observations and particle tracking simulations, *Phys. Fluids A*, *5*, 1558–1574, 1993.

Weast, R. C., and M. J. Astle (Eds.), *Handbook of Chemistry and Physics*, 61st ed., pp. 227–276, CRC, Boca Raton, Fla., 1980.

Welty, C., and L. W. Gelhar, Stochastic analysis of the effects of fluid density and viscosity variability on macrodispersion in heterogeneous porous media, *Water Resour. Res.*, *27*, 2061–2075, 1991.

P. Berest, J. P. Hulin, V. Kretz, and D. Salin, Laboratoire FAST, Bâtiment 502, Campus Paris-Sud, 91405 Orsay, France. (dos@fast.u-psud. fr)